

# Affostruction: 3D Affordance Grounding with Generative Reconstruction

Chunghyun Park  
POSTECH

p0125ch@postech.ac.kr

Seunghyeon Lee  
Ewha Womans University

2277044@ewha.ac.kr

Minsu Cho  
POSTECH, RLWRLD

mscho@postech.ac.kr

## Abstract

*This paper addresses the problem of affordance grounding from RGBD images of an object, which aims to localize surface regions corresponding to a text query that describes an action on the object. While existing methods predict affordance regions only on visible surfaces, we propose Affostruction, a generative framework that reconstructs complete geometry from partial observations and grounds affordances on the full shape including unobserved regions. We make three core contributions: generative multi-view reconstruction via sparse voxel fusion that extrapolates unseen geometry while maintaining constant token complexity, flow-based affordance grounding that captures inherent ambiguity in affordance distributions, and affordance-driven active view selection that leverages predicted affordances for intelligent viewpoint sampling. Affostruction achieves 19.1 aIoU on affordance grounding (40.4% improvement) and 32.67 IoU for 3D reconstruction (67.7% improvement), enabling accurate affordance prediction on complete shapes.*

## 1. Introduction

Robotic manipulation requires understanding not only what kinds of objects a robot observes, but also how it can use them. In the literature, such functional properties that objects can offer—affordances—are typically predicted from complete 3D shapes [4, 28, 44]. Real-world robots, however, observe objects through RGBD cameras from limited viewpoints, resulting in partial observations with significant occlusions. Recent methods address partial observations [4, 11, 50], but predict affordances only on visible surfaces. This limitation raises a critical issue in real-world situations: a robot viewing a mug from the front needs to reason about the occluded handle for grasping. Existing work on open-vocabulary affordance grounding from RGBD [30, 31, 34, 38] operates directly on partial point clouds, limiting predictions to observed surfaces, while methods for 3D reconstruction from multi-view images [10, 26, 39, 42, 43, 48] can complete geometry but

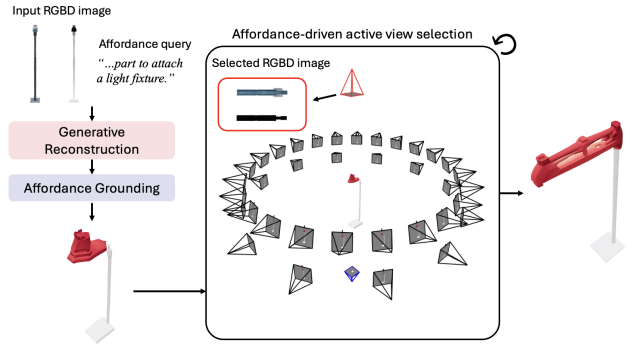


**Figure 1. Affostruction.** Given an initial RGBD observation where functional regions for an affordance query (e.g., “attach a light fixture”) are poorly visible, we perform generative reconstruction to complete the 3D geometry and predict affordances on the full shape including occluded surfaces using flow-based grounding. Our affordance-driven active view selection identifies optimal viewpoints (red) that maximize visibility of high-affordance regions while avoiding ineffective views (blue), prioritizing observation of functional regions during multi-view capture.

lack mechanisms for grounding functional affordances.

The core insight of our work is that affordance grounding on complete geometry requires first reconstructing the full shape from partial observations. Understanding where the mug handle is—and how to grasp it—requires extrapolating the occluded geometry. This motivates our approach: generating complete geometry enables affordance prediction on surfaces that were never directly observed.

In this work, we introduce **Affostruction**, a generative framework that reconstructs complete geometry from partial observations and grounds affordances on the full shape including unobserved regions. Our approach is motivated by two key observations. First, robotic scenarios naturally provide multi-view RGBD sequences as cameras move or objects are manipulated. We leverage this through sparse voxel fusion of DINOv2 [33] features that generates complete geometry by extrapolating unseen regions, aggregating information from multiple views while maintaining constant computational complexity. Second, affordances are ambiguous—multiple valid distributions exist for the same

query (e.g., “grasp”). We address this through flow-based generation, learning distributions over affordance heatmaps rather than deterministic predictions. This probabilistic formulation naturally captures multi-modal nature of functional interactions, providing richer affordance understanding.

We build upon TRELLIS [20], a foundation model for 3D generation. TRELLIS provides a strong prior for completing 3D structures from sparse observations, trained on large-scale 3D datasets. However, it lacks the ability to process multi-view RGBD inputs and ground functional affordances, limiting its application to robotic manipulation scenarios. We extend TRELLIS with two key components: multi-view sparse voxel fusion that aggregates DINOv2 features conditioned on depth, and a flow-based affordance module that generates heatmaps from text queries. The sparse voxel representation maintains constant token complexity regardless of view count, enabling efficient aggregation. These extensions enable affordance understanding on complete geometry from multi-view RGBD images while leveraging the foundation model’s geometric priors.

Our contributions are as follows:

- **Generative multi-view reconstruction:** We propose sparse voxel fusion of DINOv2 features conditioned on depth, enabling constant-complexity generative reconstruction that extrapolates unseen geometry from partial RGBD observations, providing complete shapes for affordance prediction on occluded regions.
- **Flow-based affordance grounding:** We introduce a flow-based generative model for affordance prediction that captures inherent ambiguity in functional interactions while conditioning on reconstructed geometry and natural language queries.
- **Affordance-driven active view selection:** We leverage predicted affordances to guide viewpoint sampling, enabling intelligent view selection that prioritizes functional regions.

## 2. Related work

**3D reconstruction.** Multi-view 3D reconstruction methods aim to accurately recover observed geometry from multiple RGBD or RGB images. Classical approaches like TSDF fusion [2, 14, 29, 32] accumulate depth measurements into volumetric representations, while learning-based methods like MVSNet [48] and its variants [5, 8, 49] improve quality through cost volume matching. Recent feed-forward models like DUS3R [43] and MAS3R [16] eliminate camera calibration requirements through learned geometric priors, achieving real-time performance crucial for robotic deployment. However, they only reconstruct observed regions without completing occluded geometry, limiting affordance grounding to visible surfaces when functional regions like

handles may lie on unseen parts of objects. MCC [45] extends this direction via self-supervised cross-view consistency, but it does not handle functional or affordance-related reasoning nor effectively leverage multi-view information during inference.

**3D generation.** Single-view 3D generation methods [7, 12, 18, 21, 22] learn to generate plausible complete shapes from limited observations. InstantMesh [46] and LGM [40] leverage multi-view diffusion to ensure geometric consistency, while recent sparse voxel generation methods like TRELLIS [20] and XCube [36] decompose the problem into structure and appearance generation. These approaches can complete unobserved regions critical for affordance grounding on full object shapes. However, most methods operate on single RGB images, and multi-view variants [17, 24, 37, 47] process  $N$  views through concatenated tokens with  $O(N)$  growth, limiting inputs to 4-6 views at reduced resolution—insufficient for accurate affordance prediction in cluttered scenes.

**3D affordance grounding.** Recent work enables open-vocabulary grounding using vision-language models: OpenNAD [30] combines 3D features with CLIP [35] embeddings, PointRefer [31] adds spatial reasoning, and Affogato [15] scales to diverse queries using Gemma3 [41]-generated annotations. These methods assume complete geometry and produce deterministic predictions, limiting their ability to capture uncertainty. Some works address partial observations [4, 15, 30], but predict affordances only on visible surfaces rather than completing occluded functional regions.

We address these limitations by combining multi-view reconstruction with generative completion through depth-guided sparse voxel fusion that maintains constant  $O(1)$  token complexity regardless of view count. This enables efficient integration of dense multi-view RGBD observations while completing unobserved regions for affordance grounding. Moreover, we employ flow-based generation to capture the inherent ambiguity in affordance distributions rather than producing single deterministic outputs.

## 3. Method

Given multi-view RGBD images, Affostruction grounds open-vocabulary affordances across complete 3D shapes via generative reconstruction. Our key insight is that affordance grounding on complete geometry requires first reconstructing the full shape: extrapolating complete geometry from partial observations enables affordance prediction on unobserved surfaces.

As illustrated in Fig. 2, our approach consists of three stages: (1) Generative multi-view reconstruction (Sec. 3.2) fuses visual features from multiple RGBD views into sparse voxels using depth and camera parameters, generating complete 3D structure by extrapolating unseen geometry. (2)

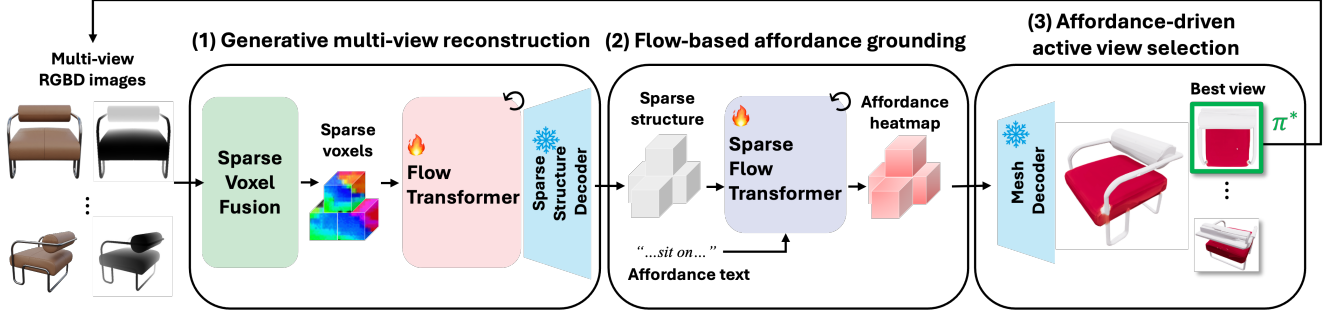


Figure 2. **Affostruction overview.** Our approach consists of three stages. (1) Generative multi-view reconstruction: DINOv2 [33] features from multiple RGBD views are fused into sparse voxels using depth and camera parameters. A Flow Transformer conditioned on these multi-view features and trained with stochastic multi-view training extrapolates complete 3D structure from partial observations, decoded via frozen sparse structure decoder [20] (left). (2) Flow-based affordance grounding: A Sparse Flow Transformer conditioned on CLIP [35]-encoded text query generates affordance heatmap logits over the reconstructed geometry (center). (3) Affordance-driven active view selection: We select next-best viewpoints by maximizing visibility of high-affordance regions, using frozen mesh decoder [20] for surface extraction (right). This enables affordance prediction on complete geometry from partial observations, with predicted affordances guiding view selection to prioritize functional regions.

Flow-based affordance grounding (Sec. 3.3) predicts affordance distributions over the reconstructed geometry conditioned on natural language queries. (3) Affordance-driven active view selection (Sec. 3.4) uses predicted affordance heatmaps to intelligently select subsequent viewpoints, prioritizing functional regions during multi-view capture.

### 3.1. Preliminaries: TRELLIS

We build upon TRELLIS [20], which decomposes 3D generation into two sequential rectified flow models [23] in sparse 3D latent space:

**Stage 1: Flow Transformer** takes a dense noise tensor  $\mathbf{X} \in \mathbb{R}^{r^3 \times C}$  (where  $r = 16$ , yielding 4096 tokens) and generates a denoised dense tensor conditioned on single RGB image condition  $\mathbf{C}$ . This denoised output is then decoded via a pretrained sparse structure VAE decoder [20] to obtain sparse structure  $\{\mathbf{p}_i\}_{i=1}^L$ , representing occupied voxel positions where  $L \ll r^3$ .

**Stage 2: Sparse Flow Transformer** operates on a sparse noise tensor initialized at predicted occupied voxels from Stage 1. It generates structured latent features  $\{\mathbf{z}_i\}_{i=1}^L$  conditioned on image features, which are then decoded via a pretrained 3D decoder (e.g., mesh, Gaussian splatting, radiance fields) [20] to produce the final 3D geometry.

Both stages are trained using the conditional flow matching (CFM) objective [19]:

$$\mathcal{L}_{\text{CFM}}(\theta) = \mathbb{E}_{t, \mathbf{X}_0, \epsilon} \left[ \|v_\theta(\mathbf{X}_t, \mathbf{C}, t) - (\epsilon - \mathbf{X}_0)\|_2^2 \right], \quad (1)$$

where  $\mathbf{X}_t = (1-t)\mathbf{X}_0 + t\epsilon$  interpolates between clean data  $\mathbf{X}_0$  and noise  $\epsilon \sim \mathcal{N}(0, I)$  with timestep  $t \in [0, 1]$ , and  $v_\theta$  predicts the velocity field.

**Limitations for affordance grounding.** TRELLIS has two key limitations for robotic manipulation: (1) it processes

only a single RGB image, precluding multi-view RGBD fusion needed for accurate reconstruction from robotic observations; (2) Sparse Flow Transformer generates visual appearance rather than functional affordances. We address these by extending Flow Transformer to support multi-view RGBD observations (Sec. 3.2) and repurposing Sparse Flow Transformer to generate affordance heatmaps (Sec. 3.3), enabling affordance grounding on complete geometry (Sec. 3.4).

### 3.2. Generative multi-view reconstruction

We extend TRELLIS’s Flow Transformer to support multi-view RGBD inputs through *multi-view sparse voxel fusion*. Rather than processing views independently, we aggregate visual features in 3D space using depth guidance before the transformer, enabling generative reconstruction that extrapolates complete geometry from partial observations. This maintains constant token complexity regardless of view count, enabling scalability and compatibility with our active view selection framework.

**Sparse voxel fusion conditioning.** We represent each view as  $\mathcal{V}_i = (I_i, D_i, K_i, T_i)$ , where  $I_i$  is an RGB image,  $D_i$  is the depth map,  $K_i$  is camera intrinsics, and  $T_i$  is camera extrinsics. For each view, we extract DINOv2 [33] features from  $I_i$  and project them to 3D space: each pixel  $(u, v)$  with depth  $d$  maps to world coordinates  $\mathbf{p} = T_i \cdot K_i^{-1} [u, v, d]^\top$ , with its DINOv2 feature  $\mathbf{f} = \text{DINOv2}(I_i(u, v))$ . This produces a sparse voxel representation  $\mathbf{V}_i = \{(\mathbf{p}_j, \mathbf{f}_j)\}_{j=1}^{L_i}$  for view  $i$ , where  $L_i$  is the number of observed voxels.

To fuse multiple views  $\{\mathcal{V}_i\}_{i=1}^N$ , we merge their sparse voxel representations. For overlapping voxels at the same position, we average their features; for non-overlapping voxels, we include them in the union. The fused representation  $\bar{\mathbf{V}} = \{(\mathbf{p}_m, \bar{\mathbf{f}}_m)\}_{m=1}^M$  is then combined with 3D po-

sitional encodings to form the final conditioning signal:

$$\mathbf{C}_{\text{voxel}} = \{\bar{\mathbf{f}}_m + \text{PE}_{3D}(\mathbf{p}_m)\}_{m=1}^M, \quad (2)$$

where  $\text{PE}_{3D}$  is a standard sinusoidal positional encoding extended to 3D voxel coordinates, concatenating separate sinusoidal encodings for each spatial dimension.

**Stochastic multi-view training.** Although TREL-LIS [20]’s cross-attention conditioning mechanism can handle varying numbers of input tokens at inference, we observe that models trained only on single views exhibit performance degradation when given multiple views. To address this, we employ stochastic multi-view training: randomly sampling 1-8 views with randomized positions during each training iteration. This enables the model to effectively leverage additional observations, showing consistent improvements as views increase, which is critical for our active view selection where observed views grow iteratively. Further analysis is provided in Sec. 4.5.

**Training objective.** We feed the conditioning signal  $\mathbf{C}_{\text{voxel}}$  to Flow Transformer [20] via cross-attention and train with the same rectified flow objective (Eq. (1)), enabling generative reconstruction that extrapolates complete sparse 3D structure from partial observations at inference.

### 3.3. Flow-based affordance grounding

Given reconstructed 3D geometry and a natural language query (e.g., “where to grasp”), we predict affordance heatmaps over the complete shape. A key challenge is that affordances are inherently ambiguous—a single query admits multiple valid interaction regions. To capture this distribution of valid affordances rather than producing a single deterministic output, we train a separate Sparse Flow Transformer from scratch to generate affordance heatmaps instead of appearance attributes.

**Text conditioning.** We encode the affordance query through a pre-trained CLIP [35] text encoder to obtain text embeddings:

$$\mathbf{C}_{\text{text}} = \text{CLIP}_{\text{text}}(q), \quad (3)$$

where  $q$  is the natural language affordance query (e.g., “where to grasp”) and  $\mathbf{C}_{\text{text}} \in \mathbb{R}^d$  serves as the conditioning signal. The affordance flow model denoises a sparse noise tensor  $\mathbf{A}_1$  initialized at the voxel positions predicted by Stage 1, conditioned on the text embedding  $\mathbf{C}_{\text{text}}$ .

**Training objective.** Following the rectified flow formulation, the model predicts velocity fields  $v_\theta$  that denoise from noise  $\epsilon \sim \mathcal{N}(0, I)$  to clean affordance logits  $\mathbf{A}_0 \in \mathbb{R}^M$  at  $M$  occupied voxels, where the noisy state  $\mathbf{A}_t = (1-t)\mathbf{A}_0 + t\epsilon$  with  $t \in [0, 1]$ . Unlike structure generation which uses MSE loss (Eq. (1)), affordance grounding requires capturing binary occupancy patterns of functional regions. We therefore define a binary mask loss that combines binary cross-entropy and Dice loss [27]:

$$\mathcal{L}_{\text{mask}}(\mathbf{A}', \mathbf{A}) = \mathcal{L}_{\text{BCE}}(\mathbf{A}', \mathbf{A}) + \mathcal{L}_{\text{Dice}}(\mathbf{A}', \mathbf{A}), \quad (4)$$

where  $\mathbf{A}'$ ,  $\mathbf{A} \in \mathbb{R}^M$  are predicted and ground truth affordance logits, respectively (sigmoid transformations are omitted for brevity but applied within BCE and Dice). This provides both point-wise supervision (BCE) and region-level optimization (Dice). The flow matching objective with binary mask loss is:

$$\mathcal{L}_{\text{CFM}}(\theta) = \mathbb{E}_{t, \mathbf{A}_0, \epsilon} [\mathcal{L}_{\text{mask}}(\epsilon - v_\theta(\mathbf{A}_t, \mathbf{C}_{\text{text}}, t), \mathbf{A}_0)]. \quad (5)$$

Only the affordance flow model is optimized while the structure generation model and text encoder remain frozen. At inference, we denoise sampled noise conditioned on text query to generate affordance logits, then apply sigmoid to obtain probability heatmaps.

### 3.4. Affordance-driven active view selection

Beyond grounding affordances on reconstructed geometry, we can leverage predicted affordance heatmaps to guide view selection. Given current observations, we select the next-best viewpoint that maximizes visibility of high-affordance regions, prioritizing functional areas during multi-view capture.

**Candidate view generation.** We generate a set of  $K = 40$  candidate camera poses  $\Pi = \{\pi_1, \dots, \pi_K\}$  uniformly distributed on a hemisphere around the target object.

**Affordance visibility metric.** Given the sparse structure with affordance heatmap  $\{(\mathbf{p}_i, a_i)\}_{i=1}^L$  from Sec. 3.3, we decode it into an affordance-colored mesh  $\mathcal{M}$  using the pre-trained TREL-LIS [20] mesh decoder. For each candidate pose  $\pi_i \in \Pi$ , we render this affordance-colored mesh  $\mathcal{M}$  to obtain a 2D image  $A_{\text{render}}$ . The affordance visibility score is simply the sum of heatmap values in the rendered image:

$$\mathcal{S}(\pi_i, \mathcal{M}) = \sum_{u,v} A_{\text{render}}(u, v), \quad (6)$$

where  $A_{\text{render}}(u, v)$  is the affordance heatmap value at pixel  $(u, v)$  in the rendered image from pose  $\pi_i$ . This metric prioritizes viewpoints that observe high-affordance regions.

**Iterative view selection.** We select the next viewpoint by maximizing the visibility score:

$$\pi^* = \arg \max_{\pi_i \in \Pi} \mathcal{S}(\pi_i, \mathcal{M}). \quad (7)$$

Starting from an initial view  $\mathcal{V}_1$ , we select the next-best pose  $\pi^*$ , capture RGBD observation  $\mathcal{V}^*$  from  $\pi^*$ , and add it to the view set. This process repeats, with affordance predictions guiding view selection to prioritize observation of functional regions.

## 4. Experiments

We evaluate Affostruction on 3D reconstruction and affordance grounding. After validating reconstruction quality (Sec. 4.2), we assess flow-based affordance grounding on complete geometry (Sec. 4.3). We then test affordance grounding from partial observations (Sec. 4.4),

Table 1. 3D reconstruction results on Toys4k.

Method	Depth	Geometry					Appearance	
		IoU $\uparrow$	CD $\downarrow$	F-score $\uparrow$	PSNR-N $\uparrow$	LPIPS-N $\downarrow$	PSNR $\uparrow$	LPIPS $\downarrow$
Shap-E [12]		6.39	0.6724	0.0096	16.16	0.3014	16.59	0.2989
InstantMesh [46]		13.68	0.4063	0.0391	20.46	0.2463	19.57	0.2382
LGM [40]		9.39	0.5660	0.0267	17.03	0.3974	13.59	0.4126
TRELLIS [20]		19.49	0.3694	0.0496	20.96	0.2089	17.61	0.2435
MCC [45]	✓	21.11	0.3299	0.0648	N/A	N/A	N/A	N/A
Affostruction (ours)	✓	<b>32.67</b>	<b>0.2427</b>	<b>0.0997</b>	<b>22.64</b>	<b>0.1421</b>	<b>18.84</b>	<b>0.1922</b>

Table 2. Complete 3D affordance grounding results on Affogato.

Method	aIoU $\uparrow$	AUC $\uparrow$	SIM $\uparrow$	MAE $\downarrow$
OpenAD [30]	3.1	64.8	0.329	0.150
PointRefer [31]	10.5	76.1	0.405	0.120
Espresso-3D [15]	13.6	<b>79.0</b>	<b>0.429</b>	<b>0.111</b>
Affostruction (ours)	<b>19.1</b>	72.0	0.426	0.217

comparing against methods that predict only on visible surfaces and two-stage reconstruction-then-affordance approaches. Ablations analyze stochastic multi-view training and affordance-driven active view selection (Sec. 4.5).

#### 4.1. Setup

**Training datasets.** Following TRELLIS [20], we train on 3D-FUTURE [6], HSSD [13], and ABO [1]. Instead of Objaverse-XL [3] which overlaps with Affogato’s source data, we use Affogato train [15] to prevent test set leakage.

**Evaluation datasets.** Following TRELLIS [20], we evaluate 3D reconstruction on 1,250 samples from Toys4k [20], a dataset of 4,000 toy objects with ground truth geometry (sampled object IDs provided in supplementary material). For affordance grounding (both complete and partial settings), we use Affogato’s test split [15]. Partial evaluation uses only the first RGBD view as input.

**Implementation details.** We train for 450k steps on 8 A100 GPUs with batch size 8 per GPU, using AdamW [25] ( $\text{lr} = 10^{-4}$ ). Visual features are extracted using DINOv2-large [33], and text queries are encoded with CLIP ViT-L/14 [35]. We use classifier-free guidance [9] with 10% unconditional dropout during training. Stochastic multi-view training samples 1-8 views per iteration.

#### 4.2. 3D reconstruction

**Metrics.** We measure geometric accuracy via volumetric IoU, Chamfer Distance (CD), and F-score ( $\tau = 0.05$ ). For appearance, we render RGB and normal images from a random view ( $r = 2$ ,  $\text{FoV} = 40^\circ$ ) and compute PSNR and LPIPS (-N suffix for normals).

**Results.** Table 1 compares reconstruction quality on Toys4k. Affostruction achieves 32.67 IoU, substantially

*“Point to the part you would use to place a book on.”*

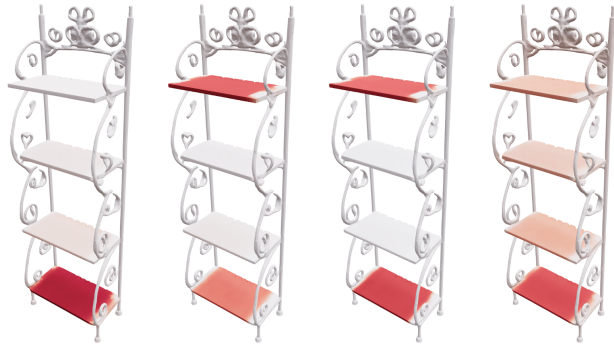


Figure 3. **Diverse affordance predictions.** Four sampling iterations for the same object-query pair produce diverse valid affordance distributions, demonstrating that our generative approach effectively captures the inherent ambiguity in affordance.

outperforming both TRELLIS [20] (19.49, +67.7%) and MCC [45] (21.10, +54.8%). While TRELLIS produces high-fidelity generations, its RGB-only approach without depth conditioning leads to inconsistencies in object orientation and scale relative to ground truth, resulting in poor geometric metrics. MCC addresses this through depth-based reconstruction, achieving better geometric accuracy than TRELLIS across IoU, CD, and F-score, though it cannot be evaluated on rendering-based metrics as it does not produce mesh outputs. Our method surpasses both approaches by effectively leveraging depth information through a flow matching-based generative framework with sparse voxel fusion. This demonstrates that depth-conditioned generation with flow matching provides stronger geometric priors for extrapolating complete shapes from partial observations compared to both RGB-only generation and discriminative depth-based methods.

#### 4.3. Complete 3D affordance grounding

**Metrics.** Following Espresso-3D [15], we report average Intersection over Union (aIoU), Area Under Curve (AUC), and Similarity (SIM) as primary metrics for comparing probability distributions. MAE measures absolute heatmap



Figure 4. **Qualitative results on partial 3D affordance grounding.** Affostruction reconstructs complete geometry and grounds affordances throughout entire objects from single RGBD views. Despite limited observations, our method predicts affordances on occluded regions, demonstrating the ability to reason about 3D functional interactions even when large portions of objects are unobserved.

values without considering annotation scale, thus serving as a secondary metric.

**Results.** Table 2 evaluates affordance grounding given complete geometry. We compare against OpenAD [30] and PointRefer [31] using their official implementations, and Espresso-3D [15] reproduced from the paper description. Unlike existing methods that fine-tune vision encoders with discriminative objectives, our generative approach produces affordance heatmaps without additional vision encoder training. While this yields slightly lower AUC (72.0 vs 79.0) and SIM, we surprisingly achieve 19.1 aIoU—40.4% better than Espresso-3D (13.6). Notably, despite not being optimized with discriminative objectives like prior methods, our generative formulation excels at precisely localizing affordance regions, as reflected in the substantial aIoU improvement. Moreover, our flow-based formulation naturally captures affordance ambiguity: multiple sampling iterations generate diverse yet valid affordance distributions for the same query (Fig. 3), demonstrating effective modeling of the inherent ambiguity in functional interactions.

#### 4.4. Partial 3D affordance grounding

**Metrics.** Unlike complete affordance grounding where predictions align with observed regions, partial settings require evaluating affordances across the entire 3D geometry—a crucial capability for robotic manipulation that needs functional understanding of complete objects beyond visible surfaces. While prior work evaluates affordances only

within observed regions using the same metrics as complete settings, we propose metrics that specifically assess the ability to predict affordances on complete 3D geometry.

We threshold both predicted and ground truth affordance point clouds at five probability levels ( $\tau \in \{0.1, 0.2, 0.3, 0.4, 0.5\}$ ) to obtain binary affordance regions. At each threshold, we compute volumetric IoU and Chamfer Distance (CD) between the thresholded point sets. We report average IoU (aIoU) and average CD (aCD) by averaging across all thresholds. This multi-threshold evaluation assesses whether methods can accurately localize functional regions throughout complete geometry, including unobserved surfaces. Formally, given predicted and ground truth affordance point clouds  $\{(\mathbf{p}_i', a_i')\}$  and  $\{(\mathbf{p}_j, a_j)\}$ :

$$\begin{aligned} \text{aIoU} &= \frac{1}{|\mathcal{T}|} \sum_{\tau \in \mathcal{T}} \text{IoU}(\mathcal{P}'_\tau, \mathcal{P}_\tau), \\ \text{aCD} &= \frac{1}{|\mathcal{T}|} \sum_{\tau \in \mathcal{T}} \text{CD}(\mathcal{P}'_\tau, \mathcal{P}_\tau), \end{aligned} \quad (8)$$

where  $\mathcal{P}_\tau = \{\mathbf{p}_i \mid a_i \geq \tau\}$  are thresholded point sets and  $\mathcal{T} = \{0.1, 0.2, 0.3, 0.4, 0.5\}$ .

These metrics jointly evaluate two critical capabilities: accurate 3D reconstruction and precise affordance localization on the reconstructed geometry. High performance requires both components to succeed—accurate reconstruction alone is insufficient if affordance predictions are poorly localized, and conversely, correct affordance understanding

Table 3. Partial 3D affordance grounding results on Affogato.

Method	Recon.	aIoU $\uparrow$	aCD $\downarrow$
OpenAD [30]		0.38	0.4165
PointRefer [31]		0.53	0.3072
Espresso-3D [15]		0.60	0.2885
TRELLIS [20] + OpenAD [30]	✓	1.49	0.1671
TRELLIS [20] + PointRefer [31]	✓	2.05	0.1576
TRELLIS [20] + Espresso-3D [15]	✓	2.23	0.1568
MCC [45] + OpenAD [30]	✓	3.34	0.1503
MCC [45] + PointRefer [31]	✓	4.19	0.1397
MCC [45] + Espresso-3D [15]	✓	4.74	0.1354
Affostruction (ours)	✓	<b>9.26</b>	<b>0.1044</b>

cannot compensate for inaccurate geometric reconstruction. This coupled evaluation reflects the practical requirements for robotic manipulation, where both complete object geometry and functional region localization must be reliable.

**Results.** Table 3 evaluates the challenging setting where affordances must be predicted on complete objects from single RGBD views. Existing affordance grounding methods—OpenAD [30], PointRefer [31], and Espresso-3D [15]—predict affordances only on observed surfaces without reconstruction. When evaluated on complete geometry using our new metrics, they achieve poor performance (0.38–0.60 aIoU) since they cannot reason about unobserved regions. Even strongest baseline, Espresso-3D (0.60 aIoU), fails to ground affordances beyond visible surfaces.

Generating complete geometry from partial observations before affordance grounding substantially improves results. We evaluate this approach using two reconstruction baselines: TRELLIS [20] (RGB input) and MCC [45] (RGBD input, matching our input modality for fair comparison). By first reconstructing the full 3D shape through unseen view generation, then applying pretrained affordance models on the complete geometry, performance increases dramatically: TRELLIS+Espresso-3D reaches 2.23 aIoU—3.7 $\times$  better than Espresso-3D alone. This demonstrates that extrapolating complete geometry is crucial for affordance prediction. However, this decoupled pipeline has fundamental limitations: reconstruction errors propagate to affordance grounding, and the two-stage approach cannot leverage affordance reasoning during the reconstruction process.

Affostruction addresses these limitations by training generative reconstruction and affordance grounding within a single framework, achieving 9.26 aIoU from a single RGBD view—4.2 $\times$  better than TRELLIS+Espresso-3D. This substantial gap demonstrates the effectiveness of our unified approach even without active view selection. Additionally, Affostruction enables affordance-driven active view selection: predicted affordances guide viewpoint sampling to prioritize functional regions. With active view selection, performance improves further: 11.17 aIoU with

2 views and 12.46 aIoU with 4 views. Figure 4 visualizes qualitative results, showing that Affostruction successfully extrapolates complete geometry and grounds affordances throughout entire objects even from challenging partial RGBD observations.

## 4.5. Ablation study

**Stochastic multi-view training benefits.** To validate the effectiveness of our sparse voxel fusion, we compare four conditioning approaches using the same Flow Transformer architecture: (1) *RGB image patches*: DINOv2 features from RGB images only, matching TRELLIS [20], (2) *RGBD image patches (DINOv2)*: depth maps replicated to 3 channels and processed through DINOv2 to create image patches, (3) *RGBD image patches (MCC)*: features from pretrained MCC [45] encoder, and (4) *Sparse voxel fusion (ours)*: multi-view DINOv2 features fused in 3D space using depth-guided projection. Each method is trained under two regimes: single-view training (using only one view per sample) and multi-view training (stochastic sampling of 1–8 views per iteration).

Figure 5 demonstrates that multi-view training is essential for exploiting additional observations to extrapolate unseen geometry. Models trained only on single views show minimal improvement or even performance degradation when given multiple inputs at inference—they cannot effectively integrate additional information for unseen view generation. In contrast, stochastic multi-view training enables consistent improvements as views increase, plateauing around 6–8 views. Affostruction achieves the best performance in both settings: with multi-view training, IoU improves from 33.32 (single view) to 46.65 (8 views), confirming that sparse voxel fusion successfully aggregates multi-view cues for accurate reconstruction.

**Affordance-driven active view selection.** We validate that affordance predictions can guide view selection to prioritize functional regions. Given an initial view, we compare three sampling strategies using Affostruction: sequential (pre-determined circular trajectory), random (uniform selection), and affordance-driven (ours, selecting views maximizing visibility of predicted high-affordance regions). To ensure a challenging evaluation, all methods start from the viewpoint with minimal affordance visibility based on ground truth.

Figure 6 shows results on the Affogato test set. All methods start from the worst viewpoint with minimal affordance visibility ( $\sim$ 4.3 aIoU). Affordance-driven view selection achieves the fastest improvement, reaching 9.2 aIoU with just one additional view—2.0 $\times$  better than sequential (4.7) and 1.5 $\times$  better than random (6.2). The advantage persists through 4 views where active view selection reaches 12.4 aIoU, substantially ahead of sequential (9.1) and random (11.0). Sequential sampling exhibits the slowest improvement due to starting from the worst view and following a

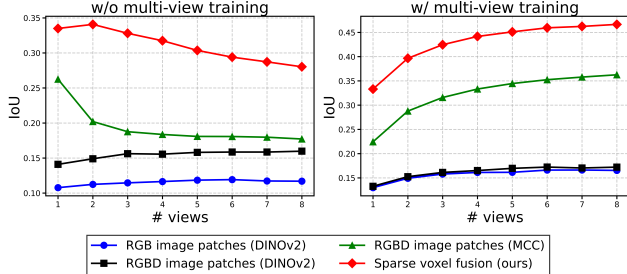


Figure 5. **Multi-view training impact.** We compare IoU (geometric reconstruction accuracy) as a function of the number of input views for methods trained with and without multi-view supervision. Methods trained on single views show minimal improvement or even degradation when given multiple views at inference (left group), while multi-view trained methods show consistent improvements with additional views (right group). Our method achieves the best performance in both settings, with multi-view training enabling effective exploitation of additional observations.

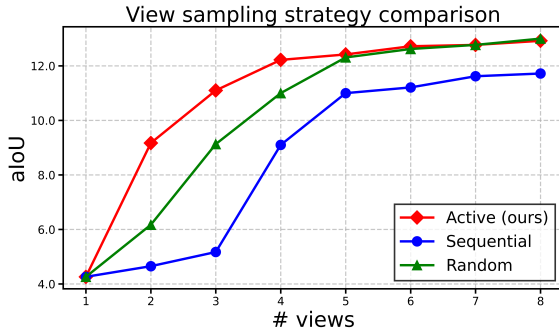


Figure 6. **Affordance-driven active view sampling.** We compare affordance grounding quality (aIoU) as views are incrementally added using different sampling strategies on the Affogato test set. All methods start from the same challenging viewpoint with poor affordance visibility. Our affordance-driven active sampling (red) achieves the fastest improvement by prioritizing viewpoints that reveal important regions. Sequential sampling (blue) shows the slowest improvement due to its predetermined trajectory. Random sampling (green) performs between the two extremes and converges with active sampling as more views are added.

predetermined trajectory that may not prioritize functional regions for unseen view generation. Random sampling performs between the two extremes, and by 5+ views begins converging toward active sampling as sufficient observations accumulate. By 8 views, active and random sampling converge to similar performance (13.3 vs 13.2 aIoU), while sequential sampling remains behind at 11.7 aIoU, demonstrating that with limited view budgets, active view selection provides substantial efficiency gains. This validates that affordance-driven view selection efficiently prioritizes functional regions, improving affordance grounding performance with limited view budgets.

## 5. Conclusion

We have presented Affostruction, a generative framework for 3D affordance grounding from RGBD images that reconstructs complete geometry and grounds affordances on the full shape including unobserved regions. Three innovations enable this approach: sparse voxel fusion for efficient multi-view reconstruction with constant computational complexity, flow-based affordance generation that naturally captures uncertainty through diverse sampling, and affordance-driven active view selection that leverages predicted heatmaps to prioritize functional regions during multi-view capture. Experiments validate substantial improvements in both affordance grounding and reconstruction quality, with affordance-driven view selection rapidly achieving accurate functional understanding from limited observations and consistently outperforming baseline strategies. Future work will extend this to multi-object scenes and explore incorporating scene-level cues to enhance affordance grounding for robotic manipulation.

## A. Implementation details

### A.1. Model architectures

Our method employs two distinct flow-based models: a Flow Transformer for multi-view 3D reconstruction (Stage 1) and a Sparse Flow Transformer for affordance grounding (Stage 2). Both models follow the rectified flow framework [20, 23] but operate on different representations and serve complementary purposes.

**Flow Transformer (Stage 1).** The Flow Transformer extends TRELLIS [20] to support multi-view RGBD inputs through sparse voxel fusion conditioning. It processes a dense noise tensor  $\mathbf{X} \in \mathbb{R}^{16^3 \times 8}$  (4096 tokens) conditioned on fused DINOv2 [33] features from multiple views. We employ the DINOv2-ViT-L/14 with registers (dino2\_vitl14\_reg) as our visual feature extractor, which produces 1024-dimensional features. See Table A1 for complete architectural specifications.

**Sparse Flow Transformer (Stage 2).** The Sparse Flow Transformer operates on sparse voxel positions predicted by Stage 1, generating affordance heatmaps conditioned on natural language queries. We use CLIP-ViT-L/14 [35] (openai/clip-vit-large-patch14) as the text encoder, producing 768-dimensional text embeddings. Unlike the dense reconstruction model, this sparse formulation processes only occupied voxels ( $L \ll 4096$ ), enabling efficient affordance prediction. Full specifications are provided in Table A2.

### A.2. Training configuration

**Common training setup.** Both models share core training parameters: 450K steps with batch size 8 per GPU, AdamW optimizer [25] (learning rate  $10^{-4}$ , no weight decay), EMA (rate 0.9999), and mixed precision (FP16) with

Table A1. **Flow Transformer Architecture (Stage 1: Multi-view Reconstruction).** The model generates dense 3D structure from multi-view RGBD observations through DINOv2 sparse voxel fusion conditioning.

Component	Value	Description
<i>Transformer Architecture</i>		
Resolution	16	Spatial resolution of dense 3D grid ( $16^3 = 4096$ tokens)
Input channels	8	Channels of input noise tensor
Output channels	8	Channels of denoised output tensor
Model channels	768	Hidden dimension of transformer blocks
Conditioning channels	1024	Dimension of DINOv2 features (ViT-L/14)
Number of blocks	12	Depth of DiT (Diffusion Transformer) backbone
Number of heads	12	Multi-head attention heads per block
MLP ratio	4	Hidden dimension multiplier for feed-forward layers
Patch size	1	Spatial patch size for tokenization
Positional encoding	APE	Absolute positional encoding
QK RMS norm	✓	RMS normalization for query-key projections
Precision	FP16	Mixed precision training with FP16
<i>Conditioning Mechanism</i>		
Visual encoder	DINOv2-ViT-L/14-reg	Feature extractor for RGBD views
Feature dimension	1024	Output dimension of DINOv2 features
Voxel resolution	16	Resolution for sparse voxel fusion
Image size	$224 \times 224$	Input image resolution for DINOv2
Max views	8	Maximum number of views during training
Fusion method	Average	Feature averaging for overlapping voxels

Table A2. **Sparse Flow Transformer Architecture (Stage 2: Affordance Grounding).** The model generates affordance heatmaps on sparse 3D structure conditioned on text queries via CLIP.

Component	Value	Description
<i>Transformer Architecture</i>		
Resolution	64	Spatial resolution for latent representation
Input channels	1	Single channel for affordance heatmap
Output channels	1	Single channel affordance prediction
Model channels	768	Hidden dimension of transformer blocks
Conditioning channels	768	Dimension of CLIP text embeddings (ViT-L/14)
Number of blocks	12	Depth of DiT backbone
Number of heads	12	Multi-head attention heads per block
MLP ratio	4	Hidden dimension multiplier for feed-forward layers
Patch size	2	Spatial patch size for tokenization
I/O residual blocks	2	Number of input/output residual blocks
I/O block channels	128	Hidden channels in I/O residual blocks
Positional encoding	APE	Absolute positional encoding
QK RMS norm	✓	RMS normalization for query-key projections
Precision	FP16	Mixed precision training with FP16
<i>Conditioning Mechanism</i>		
Text encoder	CLIP-ViT-L/14	Text feature extractor (openai/clip-vit-large-patch14)
Feature dimension	768	Output dimension of CLIP text embeddings

adaptive gradient clipping (max norm 1.0, 95th percentile). Timestep  $t$  is sampled from a logit-normal distribution ( $\mu = 1.0, \sigma = 1.0$ ). We apply 10% unconditional training for classifier-free guidance [9].

**Stage 1: Multi-view reconstruction.** The reconstruction model uses MSE loss and validates on Toys4k [20] (primary metric: MSE). Training employs stochastic multi-view sampling (1-8 views) to ensure robust fusion at inference.

**Stage 2: Affordance grounding.** The affordance model employs combined binary cross-entropy and Dice loss to capture binary patterns. We use elastic training with a linear memory controller (target ratio 0.75) for variable structure sizes. Noise scale is set to 5.0 for binary heatmaps. Validation uses Affogato [15] (primary metric: average IoU).

### A.3. Evaluation configuration

**3D reconstruction on Toys4k [20].** Following TREL-LIS [20], we evaluate reconstruction quality on 1,250 randomly selected samples (SHA256 identifiers in Table A3). For image metrics, we render both ground truth and predictions from a fixed viewpoint (radius  $r = 2.0$ , FOV 40, resolution  $512 \times 512$ ) to compute PSNR and LPIPS. For point cloud metrics (Chamfer Distance and F-score), we render depth maps from 100 views uniformly distributed via Hammersley sampling, unproject to 3D coordinates, and sample 100K points.

**Affordance grounding on Affogato [15].** We evaluate on the entire test split, following standard protocol: first view and first query per sample. Since our method is generative, we use noise scale 0.5 (instead of training scale 5.0) for stable quantitative results.

## B. Sampling parameters search

We investigate the optimal number of sampling steps for our multi-view reconstruction model. Figure A1 shows volumetric IoU across different sampling steps (1, 5, 10, 15, 20) and number of input views (1-6). Our analysis reveals that reconstruction quality plateaus at 5 sampling steps regardless of the number of views. Beyond this point, additional steps yield negligible improvement while significantly increasing inference time. At 5 steps, our model achieves a sampling time of approximately 0.25 seconds, which is  $5 \times$  faster than the 25-step sampling (1.29s) used by TREL-LIS [20]. This efficiency is particularly important for our iterative reconstruction-affordance cycle, where rapid reconstruction enables real-time active view selection for robotic applications.

## C. Additional qualitative results

**Progressive improvement through reconstruction-affordance cycle.** Figure A2 illustrates the iterative

refinement process from challenging initial observations. We deliberately select starting viewpoints where target functional areas have minimal visibility, creating difficult scenarios. Through iterative cycles of generative reconstruction, affordance prediction, and active view selection, both geometric quality and localization precision progressively improve. The visualizations reveal mutual reinforcement: better geometry enables more accurate predictions, which guide view selection to further enhance reconstruction quality. This validates our core insight—these tasks are not independent but form a synergistic cycle where each component benefits the other.

### Additional qualitative results on diverse affordances.

Figure A3 demonstrates Affostruction’s ability to predict affordances on complete 3D objects from partial RGBD observations across diverse categories and queries. The visualizations span various affordance types (e.g., “cut”, “swing”, “carry”), where our method successfully identifies functional areas throughout entire objects, including occluded surfaces. Notably, predictions extend to unobserved regions invisible from input views, validating that our framework effectively leverages reconstructed geometry for holistic reasoning beyond visible surfaces. Strong generalization across categories and queries confirms robustness in real-world scenarios with limited observations.

Table A3. **Toys4k test set samples (SHA256 identifiers).** The 1,250 samples used for 3D reconstruction evaluation, following TREL-LIS [20]. Full list available in `toys4k.test_ids.txt`. Hashes truncated to first 12 characters for display.

SHA256 Object Identifiers (1,250 samples)				
000a283e3a4e...	002d00832905...	0036c7bf5fa3...	00b614f80a13...	0100555a135f...
016be2974e32...	019335038b79...	01a79ca24eac...	01ac5979fed3...	02065cccd7123...
021c0a67be93...	0262655e3219...	0268f36995da...	0289dd8d108d...	0290334c3684...
02a87d37f648...	02ba6532f9de...	02c70213d5af...	02e84388b24c...	02e9faa6bff3...
... (1,230 additional samples)				

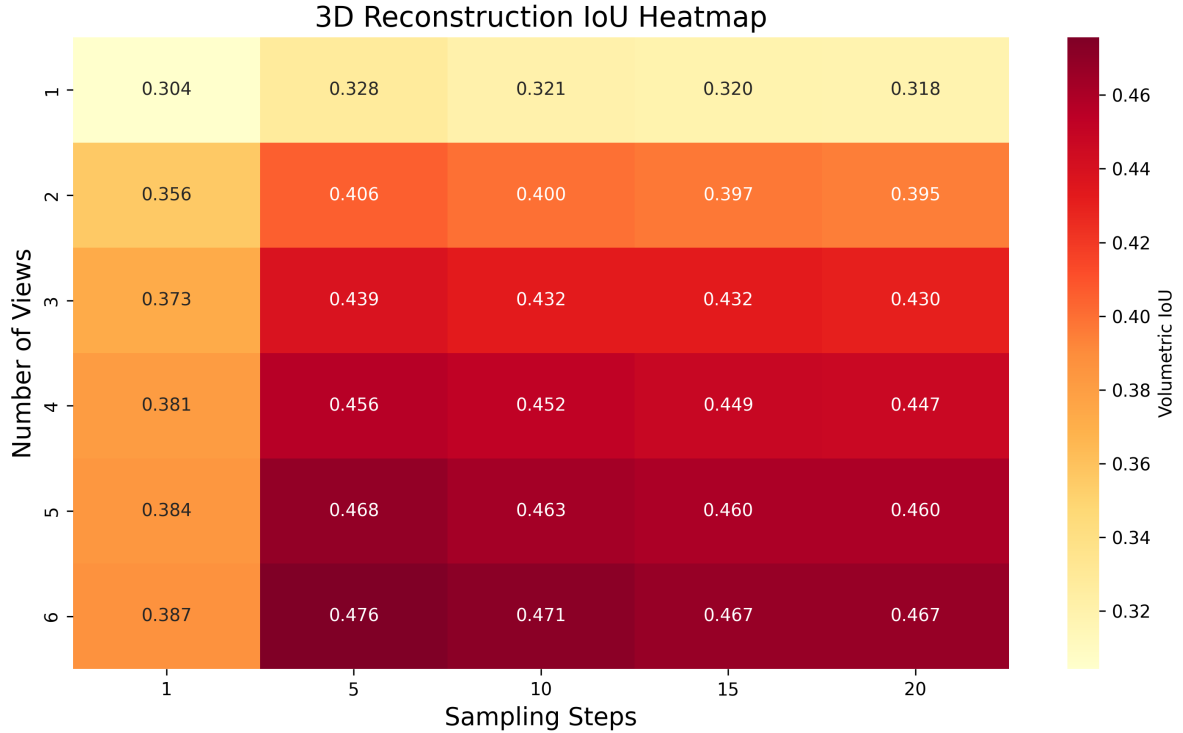
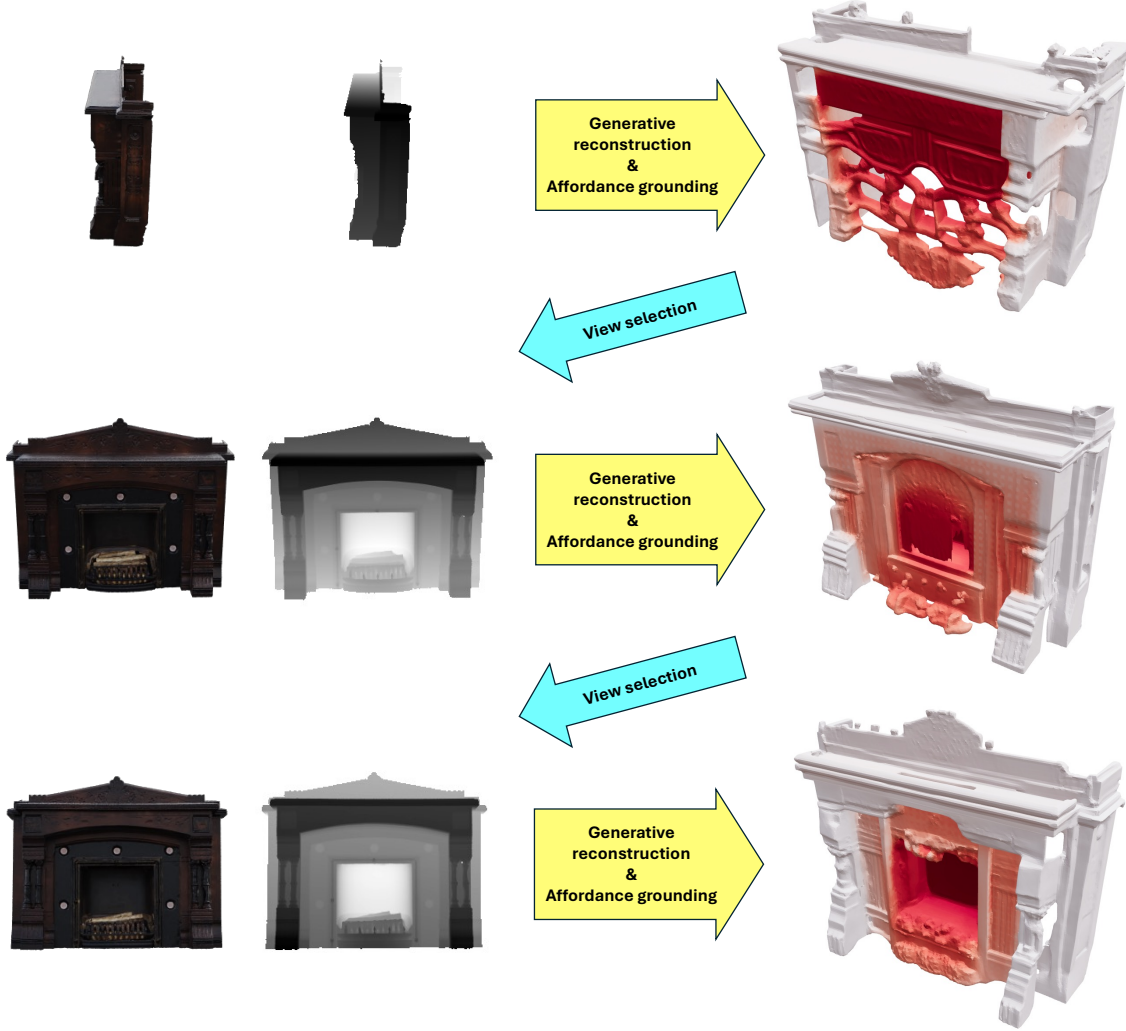


Figure A1. **Sampling step ablation across different number of views.** We evaluate volumetric IoU for varying sampling steps (1, 5, 10, 15, 20) with 1–6 input views. Reconstruction quality saturates at 5 steps across all view configurations, achieving 5× faster sampling (0.25s) compared to the default 25 steps in TREL-LIS [20].

*“Point to the part you would place logs in.”*



**Figure A2. Progressive improvement through the reconstruction-affordance cycle.** Starting from challenging viewpoints where target areas are barely visible, Affostruction progressively refines geometry and localization through an iterative cycle: (1) generative reconstruction extrapolates complete structure from partial observations, (2) affordance prediction on reconstructed geometry, and (3) active view selection targeting informative viewpoints. Each iteration improves both reconstruction quality and prediction accuracy, revealing the synergistic relationship between these tasks. While only the selected view is shown for clarity, subsequent iterations leverage all accumulated observations through multi-view fusion.

Input RGBD image



Affordance grounding on the reconstructed 3D shapes



*“Point to the edge you would use to cut.”*



*“Point to the part you would hold to swing.”*



*“Point to the part you would rest your arm on.”*



*“Point to the part you would lean against for support.”*



*“Point to the part you would sit on.”*



*“Point to the part you would use to support your feet.”*



*“Point to the handle you would use to carry it.”*



*“Point to the sign indicating a hazard.”*

Figure A3. **Additional qualitative results on partial 3D affordance grounding.** Affostruction predicts diverse affordances (cut, swing, carry, etc.) throughout complete objects from partial RGBD observations. Each row shows a different object-query pair, with predictions spanning both visible and occluded surfaces. Results confirm that our framework effectively leverages reconstructed geometry for holistic reasoning beyond observed regions.

## References

[1] Jasmine Collins, Shubham Goel, Kenan Deng, Achleshwar Luthra, Leon Xu, Erhan Gundogdu, Xi Zhang, Tomas F Yago Vicente, Thomas Dideriksen, Himanshu Arora, et al. Abo: Dataset and benchmarks for real-world 3d object understanding. In *Proceedings of the IEEE/CVF conference on computer vision and pattern recognition*, pages 21126–21136, 2022. 5

[2] Angela Dai, Matthias Nießner, Michael Zollhöfer, Shahram Izadi, and Christian Theobalt. Bundlefusion: Real-time globally consistent 3d reconstruction using on-the-fly surface reintegration. *ACM Transactions on Graphics (ToG)*, 36(4):1, 2017. 2

[3] Matt Deitke, Ruoshi Liu, Matthew Wallingford, Huong Ngo, Oscar Michel, Aditya Kusupati, Alan Fan, Christian Laforte, Vikram Voleti, Samir Yitzhak Gadre, et al. Objaverse-xl: A universe of 10m+ 3d objects. *Advances in Neural Information Processing Systems*, 36:35799–35813, 2023. 5

[4] Shengheng Deng, Xun Xu, Chaozheng Wu, Ke Chen, and Kui Jia. 3d affordancenet: A benchmark for visual object affordance understanding. In *IEEE/CVF Conference on Computer Vision and Pattern Recognition (CVPR)*, pages 1778–1787, 2021. 1, 2

[5] Yikang Ding, Wentao Yuan, Qingtian Zhu, Haotian Zhang, Xiangyue Liu, Yuanjiang Wang, and Xiao Liu. Transmvsnet: Global context-aware multi-view stereo network with transformers. In *Proceedings of the IEEE/CVF conference on computer vision and pattern recognition*, pages 8585–8594, 2022. 2

[6] Huan Fu, Rongfei Jia, Lin Gao, Mingming Gong, Binqiang Zhao, Steve Maybank, and Dacheng Tao. 3d-future: 3d furniture shape with texture. *International Journal of Computer Vision*, 129(12):3313–3337, 2021. 5

[7] Jun Gao, Tianchang Shen, Zian Wang, Wenzheng Chen, Kangxue Yin, Daiqing Li, Or Litany, Zan Gojcic, and Sanja Fidler. Get3d: A generative model of high quality 3d textured shapes learned from images. *Advances in neural information processing systems*, 35:31841–31854, 2022. 2

[8] Xiaodong Gu, Zhiwen Fan, Siyu Zhu, Zuozhuo Dai, Feitong Tan, and Ping Tan. Cascade cost volume for high-resolution multi-view stereo and stereo matching. In *IEEE Conference on Computer Vision and Pattern Recognition (CVPR)*, pages 2495–2504, 2020. 2

[9] Jonathan Ho and Tim Salimans. Classifier-free diffusion guidance. In *NeurIPS 2021 Workshop on Deep Generative Models and Downstream Applications*, 2021. 5, 3

[10] Shun Iwase, Katherine Liu, Vitor Guizilini, Adrien Gaidon, Kris Kitani, Rareş Ambruş, and Sergey Zakharov. Zero-shot multi-object scene completion. In *European Conference on Computer Vision*, pages 96–113. Springer, 2024. 1

[11] Zhenyu Jiang, Yifeng Zhu, Maxwell Svetlik, Kuan Fang, and Yuke Zhu. Synergies between affordance and geometry: 6-dof grasp detection via implicit representations. In *Robotics: Science and Systems (RSS)*, 2021. 1

[12] Heewoo Jun and Alex Nichol. Shap-e: Generating conditional 3d implicit functions. *arXiv preprint arXiv:2305.02463*, 2023. 2, 5

[13] Mukul Khanna, Yongsen Mao, Hanxiao Jiang, Sanjay Haresh, Brennan Shacklett, Dhruv Batra, Alexander Clegg, Eric Undersander, Angel X Chang, and Manolis Savva. Habitat synthetic scenes dataset (hssd-200): An analysis of 3d scene scale and realism tradeoffs for objectgoal navigation. In *Proceedings of the IEEE/CVF Conference on Computer Vision and Pattern Recognition*, pages 16384–16393, 2024. 5

[14] Matthew Klingensmith, Ivan Dryanovski, Siddhartha Srinivas, and Jianxiong Xiao. Chisel: Real time large scale 3d reconstruction onboard a mobile device using spatially hashed signed distance fields. In *Robotics: Science and Systems (RSS)*, 2015. 2

[15] Junha Lee, Eunha Park, Chunghyun Park, Dahyun Kang, and Minsu Cho. Affogato: Learning open-vocabulary affordance grounding with automated data generation at scale. *arXiv preprint arXiv:2506.12009*, 2025. 2, 5, 6, 7, 3

[16] Vincent Leroy, Yohann Cabon, and Jerome Revaud. Grounding image matching in 3d with mast3r. In *arXiv preprint arXiv:2406.09756*, 2024. 2

[17] Zhiqi Li, Yiming Chen, Lingzhe Zhao, and Peidong Liu. Mvcontrol: Adding conditional control to multi-view diffusion for controllable text-to-3d generation. *arXiv preprint arXiv:2311.14494*, 2023. 2

[18] Chen-Hsuan Lin, Jun Gao, Luming Tang, Towaki Takikawa, Xiaohui Zeng, Xun Huang, Karsten Kreis, Sanja Fidler, Ming-Yu Liu, and Tsung-Yi Lin. Magic3d: High-resolution text-to-3d content creation. In *Proceedings of the IEEE/CVF conference on computer vision and pattern recognition*, pages 300–309, 2023. 2

[19] Yaron Lipman, Ricky TQ Chen, Heli Ben-Hamu, Maximilian Nickel, and Matthew Le. Flow matching for generative modeling. In *The Eleventh International Conference on Learning Representations*. 3

[20] Jianfeng Liu, Xiaoshui Zeng, Zeyuan Wu, Yujun Lu, Yuan Li, Ming-Hsuan Chen, and Song-Hai Zhang. Structured 3d latents for scalable and versatile 3d generation. *arXiv preprint arXiv:2412.01506*, 2024. 2, 3, 4, 5, 7, 1

[21] Minghua Liu, Chao Xu, Haian Jin, Linghao Chen, Mukund Varma T, Zexiang Xu, and Hao Su. One-2-3-45: Any single image to 3d mesh in 45 seconds without per-shape optimization. *Advances in Neural Information Processing Systems*, 36:22226–22246, 2023. 2

[22] Ruoshi Liu, Rundi Wu, Basile Van Hoorick, Pavel Tokmakov, Sergey Zakharov, and Carl Vondrick. Zero-1-to-3: Zero-shot one image to 3d object. In *Proceedings of the IEEE/CVF international conference on computer vision*, pages 9298–9309, 2023. 2

[23] Xingchao Liu, Chengyue Gong, et al. Flow straight and fast: Learning to generate and transfer data with rectified flow. In *The Eleventh International Conference on Learning Representations*. 3, 1

[24] Yuan Liu, Cheng Lin, Zijiao Zeng, Xiaoxiao Long, Lingjie Liu, Taku Komura, and Wenping Wang. Syncdreamer: Generating multiview-consistent images from a single-view image. *arXiv preprint arXiv:2309.03453*, 2023. 2

[25] Ilya Loshchilov and Frank Hutter. Decoupled weight decay regularization. In *International Conference on Learning Representations*, 2019. 5, 1

[26] Xiaoxu Meng, Weikai Chen, and Bo Yang. Neat: Learning neural implicit surfaces with arbitrary topologies from multi-view images. In *IEEE Conference on Computer Vision and Pattern Recognition (CVPR)*, pages 3034–3043, 2023. 1

[27] Fausto Milletari, Nassir Navab, and Seyed-Ahmad Ahmadi. V-net: Fully convolutional neural networks for volumetric medical image segmentation. In *2016 fourth international conference on 3D vision (3DV)*, pages 565–571. Ieee, 2016. 4

[28] Kaichun Mo, Leonidas J Guibas, Mustafa Mukadam, Abhinav Gupta, and Shubham Tulsiani. Where2act: From pixels to actions for articulated 3d objects. In *IEEE International Conference on Computer Vision (ICCV)*, pages 6813–6823, 2021. 1

[29] Richard A Newcombe, Shahram Izadi, Otmar Hilliges, David Molyneaux, David Kim, Andrew J Davison, Pushmeet Kohi, Jamie Shotton, Steve Hodges, and Andrew Fitzgibbon. Kinectfusion: Real-time dense surface mapping and tracking. In *IEEE International Symposium on Mixed and Augmented Reality (ISMAR)*, pages 127–136. IEEE, 2011. 2

[30] Toan Nguyen, Minh Nhat Vu, An Vuong, Dzung Nguyen, Thieu Vo, Ngan Le, and Anh Nguyen. Open-vocabulary affordance detection in 3d point clouds. In *IEEE/RSJ International Conference on Intelligent Robots and Systems (IROS)*, pages 5692–5698. IEEE, 2023. 1, 2, 5, 6, 7

[31] Toan Nguyen, Minh Nhat Vu, Baoru Huang, Tuan Van Vo, Vy Truong, Ngan Le, Thieu Vo, Bac Le, and Anh Nguyen. Language-conditioned affordance-pose detection in 3d point clouds. In *IEEE International Conference on Robotics and Automation (ICRA)*, pages 4216–4223, 2024. 1, 2, 5, 6, 7

[32] Helen Oleynikova, Zachary Taylor, Marius Fehr, Roland Siegwart, and Juan Nieto. Voxblox: Incremental 3d euclidean signed distance fields for on-board mav planning. *IEEE/RSJ International Conference on Intelligent Robots and Systems (IROS)*, pages 1366–1373, 2017. 2

[33] Maxime Oquab, Timothée Darcet, Théo Moutakanni, Huy V Vo, Marc Szafraniec, Vasil Khalidov, Pierre Fernandez, Daniel HAZIZA, Francisco Massa, Alaaeldin El-Nouby, et al. Dinov2: Learning robust visual features without supervision. *Transactions on Machine Learning Research*. 1, 3, 5

[34] Shengyi Qian, Weifeng Chen, Min Bai, Xiong Zhou, Zhuowen Tu, and Li Erran Li. Affordancellm: Grounding affordance from vision language models. In *IEEE/CVF Conference on Computer Vision and Pattern Recognition Workshops (CVPRW)*, pages 5627–5637, 2024. 1

[35] Alec Radford, Jong Wook Kim, Chris Hallacy, Aditya Ramesh, Gabriel Goh, Sandhini Agarwal, Girish Sastry, Amanda Askell, Pamela Mishkin, Jack Clark, et al. Learning transferable visual models from natural language supervision. In *International conference on machine learning*, pages 8748–8763. PMLR, 2021. 2, 3, 4, 5, 1

[36] Jiakai Ren, Zehuan Liang, Xiang Feng, Yu-Guan Hwang, Yan-Pei Chen, Zeqi Liu, Xin Zhou, Chen Cao, Pan Gao, and Tobias Ritschel. Xcube: Large-scale 3d generative modeling using sparse voxel hierarchies. In *IEEE Conference on Computer Vision and Pattern Recognition (CVPR)*, pages 7309–7318, 2024. 2

[37] Yichun Shi, Peng Wang, Jianglong Ye, Mai Long, Kejie Li, and Xiao Yang. Mvdream: Multi-view diffusion for 3d generation. *arXiv preprint arXiv:2308.16512*, 2023. 2

[38] Heng Su, Mengying Xie, Nieqing Cao, Yan Ding, Beichen Shao, Xianlei Long, Fuqiang Gu, and Chao Chen. Oval-fields: Weakly supervised open-vocabulary affordance fields for robot operational part detection. In *Proceedings of the IEEE/CVF International Conference on Computer Vision*, pages 6385–6395, 2025. 1

[39] Jiaming Sun, Yiming Xie, Linghao Chen, Xiaowei Zhou, and Hujun Bao. Neuralrecon: Real-time coherent 3d reconstruction from monocular video. In *Proceedings of the IEEE/CVF conference on computer vision and pattern recognition*, pages 15598–15607, 2021. 1

[40] Jiaxiang Tang, Zhaoxi Ren, Hang Zhou, Ziwei Liu, and Gang Zeng. Lgm: Large multi-view gaussian model for high-resolution 3d content creation. In *European Conference on Computer Vision (ECCV)*, pages 381–399, 2024. 2, 5

[41] Gemma Team, Aishwarya Kamath, Johan Ferret, Shreya Pathak, Nino Vieillard, Ramona Merhej, Sarah Perrin, Tatiana Matejovicova, Alexandre Ramé, Morgane Rivière, et al. Gemma 3 technical report. *arXiv preprint arXiv:2503.19786*, 2025. 2

[42] Peng Wang, Lingjie Liu, Yuan Liu, Christian Theobalt, Taku Komura, and Wenping Wang. Neus: Learning neural implicit surfaces by volume rendering for multi-view reconstruction. In *Advances in Neural Information Processing Systems (NeurIPS)*, pages 27171–27183, 2021. 1

[43] Shuzhe Wang, Vincent Leroy, Yohann Cabon, Boris Chidlovskii, and Jerome Revaud. Dust3r: Geometric 3d vision made easy. In *IEEE Conference on Computer Vision and Pattern Recognition (CVPR)*, pages 20697–20709, 2024. 1, 2

[44] Yian Wang, Ruihai Wu, Kaichun Mo, Jiaqi Ke, Qingnan Fan, Leonidas J Guibas, and Hao Dong. Adaafford: Learning to adapt manipulation affordance for 3d articulated objects via few-shot interactions. In *European Conference on Computer Vision (ECCV)*, pages 90–107, 2022. 1

[45] Chao-Yuan Wu, Justin Johnson, Jitendra Malik, Christoph Feichtenhofer, and Georgia Gkioxari. Multiview compressive coding for 3d reconstruction. In *Proceedings of the IEEE/CVF Conference on Computer Vision and Pattern Recognition*, pages 9065–9075, 2023. 2, 5, 7

[46] Jiale Xu, Weihao Cheng, Yiming Gao, Xintao Wang, Shenghua Gao, and Ying Shan. Instantmesh: Efficient 3d mesh generation from a single image with sparse-view large reconstruction models. In *arXiv preprint arXiv:2404.07191*, 2024. 2, 5

[47] Yunhan Yang, Yukun Huang, Xiaoyang Wu, Yuan-Chen Guo, Song-Hai Zhang, Hengshuang Zhao, Tong He, and Xihui Liu. Dreamcomposer: Controllable 3d object generation via multi-view conditions. In *Proceedings of the IEEE/CVF Conference on Computer Vision and Pattern Recognition*, pages 8111–8120, 2024. 2

- [48] Yao Yao, Zixin Luo, Shiwei Li, Tian Fang, and Long Quan. Mvsnet: Depth inference for unstructured multi-view stereo. In *Proceedings of the European conference on computer vision (ECCV)*, pages 767–783, 2018. [1](#), [2](#)
- [49] Yao Yao, Zixin Luo, Shiwei Li, Tianwei Shen, Tian Fang, and Long Quan. Recurrent mvsnet for high-resolution multi-view stereo depth inference. In *IEEE Conference on Computer Vision and Pattern Recognition (CVPR)*, pages 5525–5534, 2019. [2](#)
- [50] He Zhu, Quyu Kong, Kechun Xu, Xunlong Xia, Bing Deng, Jieping Ye, Rong Xiong, and Yue Wang. Grounding 3d object affordance with language instructions, visual observations and interactions. In *IEEE/CVF Conference on Computer Vision and Pattern Recognition (CVPR)*, 2025. [1](#)